Optimizing the Incorporation of Silica Nanoparticles in Polysulfone/Poly(vinyl alcohol) Membranes with Response Surface Methodology

Law Yong Ng,[1] Choe Peng Leo,[2] Abdul Wahab Mohammad[1]

[1]*Scale-Up and Downstream Processing Research Group, Department of Process and Chemical Engineering, Faculty of Engineering and Built Environment, Universiti Kebangsaan Malaysia, 43600 Bangi, Selangor, Malaysia*
[2]*School of Chemical Engineering, Engineering Campus, Universiti Sains Malaysia, 14300 Nibong Tebal, Seberang Perai Selatan, Pulau Pinang, Malaysia*

Received 10 June 2010; accepted 21 October 2010
DOI 10.1002/app.33628
Published online 8 March 2011 in Wiley Online Library (wileyonlinelibrary.com).

ABSTRACT: The addition of silica nanoparticles and poly(vinyl alcohol) (PVA) to polysulfone (PSF) membranes was used to modify the membrane morphology and enhance membrane performance. The central composite design of the response surface methodology was used to predict the maximum permeability and real salt rejection (R_{real}) of the PSF membranes. The factors affecting the permeability and R_{real} values of the PSF membranes were the silica (0–12 wt % PSF) and PVA (0–2 wt % PSF) contents. The optimized responses, membrane permeability, and R_{real} obtained experimentally were 61.9260 L m^{-2} h^{-1} bar^{-1} and 97.5850%, respectively, with deviation from the predicted values of 34.72 and 15.84%, respectively. In the further characterization, the contact angle results showed that PVA was important in stabilizing the nanoparticle surfaces to prevent agglomeration in the polymeric matrix. The tensile strength test confirmed that the addition of silica nanoparticles improved the mechanical strength of the PSF membranes. However, the addition of PVA had a weakening effect on the mechanical strength of the PSF membranes. The addition of silica nanoparticles and PVA affected the typical asymmetric structures of the PSF membrane less, as shown in the scanning electron micrographs. This may have been due to the good incorporation of additives in the PSF membranes, as observed from the energy-dispersive X-ray and Fourier transform infrared spectroscopy results. J Appl Polym Sci 121: 1804–1814, 2011

Key words: additives; mechanical properties; membranes; morphology; nanocomposites

INTRODUCTION

Among polymeric materials, polysulfone (PSF) is one of the ideal polymeric materials for membrane fabrication because of its high mechanical properties, good heat and aging resistance, and high chemical stability.[1–4] These advantages allow PSF membranes to be widely used in diverse fields, such as wastewater or water treatment,[5,6] food processing, and biotechnology.[7] However, PSF membranes are prone to fouling because of their high hydrophobicity.[1] This problem severely limits the long-term use of these membranes in many filtration systems. Thus, it is desirable to use a polymeric membrane with a hydrophilic surface that requires the use of a wetting agent. A wide range of evidence has shown that membranes with a greater degree of hydrophilicity have an increased resistance to fouling.[8]

Various methods have been introduced to increase the performances of PSF membranes. For instance, PSF membranes have been modified by the addition of zinc chloride, which caused an increase in the rejection rate and molecular weight cutoff value,[9] and by the sulfonation method, which increased the membrane permeation flux and separation factor.[10] Other authors have reported the addition of sulfonated poly(ether ether ketone) to PSF membranes, which resulted in the membranes exhibiting a high permeability and a high rejection of dextran and sodium chloride.[8] The performance of PSF membranes has also been improved by ammonia plasma treatment.[11]

The addition of inorganic particles is also a viable option and has aroused great interest, especially[12,13] because of the convenient operation, mild conditions, and good and stable performances of PSF membranes modified by this method.[14] Composite membrane materials formed by the blending of nanosized inorganic and organic materials are attractive for the purposes of creating new materials with

Correspondence to: A. W. Mohammad (wahabm@vlsi.eng.ukm.my).

Contract grant sponsor: Universiti Kebangsaan Malaysia; contract grant number: UKM-GUP-KPB-08-32-129.

Contract grant sponsor: MOSTI; contract grant number: 02-01-02-SF0529.

new or enhanced properties, such as high permselectivity, good hydrophilicity, and excellent fouling resistance, compared with those formed with single organic or inorganic membranes.[15,16]

In this study, we modified PSF membranes by the incorporation of silica nanoparticles. A water-soluble, poly(vinyl alcohol) (PVA), was also added to the PSF membrane as a pore former and to stabilize the silica nanoparticle surfaces to encourage their dispersion in the casting solution. It was reported that the addition of silica nanoparticles, which has opposing properties compared to porous inorganic fillers, can alter the polymer chain packing in glassy, high-free-volume polymers. This results in an increase in the free volume and leads to a significant enhancement in the permeability.[17] The incorporation of silica nanoparticles in polymeric membranes can significantly increase the number of pores and the pore radius, and they are more thermally stable compared to only polymeric membranes.[18] The excellent properties of PVA, including its high hydrophilicity, flexibility, and chemical stability, are also believed to be capable of improving the performance of PSF membranes.[19]

To optimize and analyze the effects of the PVA and the silica nanoparticle content on the membrane permeability and salt rejection, a statistically designed experiment with minimum experimental runs is greatly needed. To date, many researchers have tried to enhance and optimize the membrane morphology and performance through a statistical approach.[20] Statistical approaches, including response surface methodology (RSM), have been used successfully to calculate the complex interaction between the independent process factors.[21] Thus, to produce a PSF membrane with an optimized performance, RSM was used in this study to illustrate the interaction between the PVA and the silica nanoparticles content in affecting the permeability and salt rejection of the membranes. We performed the analysis by using the central composite design (CCD) of RSM. We also evaluated the PSF membranes by measuring the tensile strength and contact angle and by using Fourier transform infrared (FTIR) spectroscopy, scanning electron microscopy (SEM), and energy-dispersive X-ray (EDX) spectroscopy.

EXPERIMENTAL

Materials

Membranes were prepared from PSF (Sigma-Aldrich, MO, molecular weight = 35,000) and PVA (Sigma-Aldrich, molecular weight = 13,000–23,000, 87–89% hydrolyzed). These polymers were blended together with the solvent 1-methyl-2-pyrrolidone (NMP), supplied from R & M Chemicals (Essex, UK). The sizes of the silica nanoparticles used were within the range 10–20 nm with a purity from trace metals of 99.5% (Sigma-Aldrich). Sodium sulfate (Na_2SO_4; Merck KGaA, 64271 Darmstadt, Germany) was used as the salt in the permeation experiment. The chemicals PSF, PVA, NMP, silica, and Na_2SO_4 were used as received without any further purification.

PSF membrane preparation

The PSF/PVA membranes incorporated with silica nanoparticles were prepared with the phase-inversion method. Casting dopes were prepared by the dissolution of PSF in the solvent NMP at a water bath temperature of 80°C with a continuous stirring rate of 500 rpm. PVA and silica nanoparticles were added slowly into the solution with continuous stirring for 5 h to create a better dispersion of nanoparticles in the solution. The casting solution was then kept in the dark for at least 24 h to release the air bubbles.

Some casting solution was poured onto a clean glass plate and dispersed with a Filmographe Doctor Blade 360099003 (Braive Instrument, Germany). The thickness of the membranes was set to 0.15 mm with the casting knife. After 15 s of exposure of the casting solution on the glass plate to the air, the glass plate was immersed in ultrapure water at room temperature for the remainder of the phase-inversion process. The membranes formed were peeled off of the glass plate and rinsed with ultrapure water for at least 30 min. Then, the membranes were stored in ultrapure water containing 1 wt % formaldehyde to prevent bacteria growth under ambient conditions.

Polymer dopes containing PSF (17 wt % of the solution) and NMP (83 wt % of the solution) were modified with different concentration of additives. Silica nanoparticles were added to the solution, with their weight percentages varying from 0 to 12 wt % PSF. Also, PVA was added to the solution, with its weight percentages varying from 0 to 2 wt % PSF. The operating ranges and the levels of the considered variables are given in Table I.

Characterization of the membranes

The membrane permeability was determined from clean water flux measurement with ultrapure water at room temperature and with a Sterlitech HP4750 (Sterlitech Corporation, WA). The dead-end filtration cell had an active membrane area (effective area) of 14.6 cm^2. The permeability of 13 membranes fabricated were tested with the dead-end filtration cell after compaction at a pressure of 16 bars. The pure water fluxes were calculated with the following equation:

$$J = \frac{V}{St}$$

TABLE I
Experimental Range and Levels of the Independent Variables

Variable	Symbol		Coded level				
	Actual	Coded	−1.414	−1.000	0	1.000	1.414
Silicon dioxide (wt %)	SiO_2	*B*	0	1.76	6.00	10.24	12.00
Poly(vinyl alcohol) (wt %)	PVA	*A*	0.00	0.29	1.00	1.71	2.00

where J is the permeate flux, V is the volume of the permeate, S is the effective membrane area, and t is the operating time.[2] The same unit was fed Na_2SO_4 salt solution at a concentration of 0.01*M* to obtain the salt rejection values of the 13 fabricated membranes. The ionic strength for the Na_2SO_4 salt was calculated to be 0.03*M*. The observed salt rejection (R_{obs}) and real salt rejection (R_{real}) results were compared at a pressure of 10 bars. The R_{obs} values are represented as R_{obs} of solute, as determined by the following equation:

$$R_{obs} = 1 - \left(\frac{C_p}{C_f}\right)$$

where C_p is the concentration of solute in the permeate and C_f is the concentration of solute in the feed stream.[22] By using the R_{obs} values, we calculated R_{real} on the basis of the following equation:

$$R_{real} = 1 - \left(\frac{C_p}{C_w}\right)$$

where C_w is the concentration of solute buildup at the wall of the membrane. The R_{real} model is one of the good predictive models used here. A good predictive model allow us to obtain membrane characteristics, predict process performance, and optimize the process.[23] For detailed calculation and the theory of R_{real}, one can refer to previous work.[24] The correlation between R_{real} and R_{obs} was used to determine the C_w value, as shown:

$$\ln\left(\frac{1-R_{obs}}{R_{obs}}\right) = \ln\left(\frac{1-R_{real}}{R_{real}}\right) + \frac{J_V}{k}$$

$$k = k'\omega^{0.567}$$

$$k' = 0.23\left(\frac{r^2}{V}\right)^{0.567}\left(\frac{V}{D_\infty}\right)^{0.33}\frac{D_\infty}{r}$$

where J_v is permeate flux of a solution at 10 bars, ω is the stirring speed, r is the radius of the membrane effective surface area, V is the kinematic viscosity, D_∞ is the diffusion coefficient for the solution, and k, k' are the mass transfer coefficient of the stirred cell.

The contact angle between water and the membrane surface was measured with a contact-angle measurement apparatus (Ramé-Hart Co., NJ) after the membranes were dried overnight.[25] The instrument used was a Ramé-Hart model 200 standard contact angle goniometer with DROPimage Standard Software with an accuracy of ±0.10°. The media used for contact angle measurement were deionized water and air at ambient temperature (22–23°C).

We conducted the tensile strength by cutting out a membrane sample in a rectangular shape, where the width and length of the membranes were 5 and 40 mm, respectively. The length of the specimen in the gauge section was 10 mm on both sides. The applied stroke speed was set to be 2 mm/min, and the test temperature was ambient temperature. The tensile strength measurements were done with an Instron 5560 (Norwood, MA) series table model testing system.

The surface and cross-sectional structures of a few of the membranes were examined by SEM. The equipment used was a Gemini model SUPRA 55VP-ZEISS (Oberkochen, Germany). The cross sections of the membranes were prepared by the fracturing of the membranes at the temperature of liquid nitrogen. All of the specimens were coated with a thin layer of gold before they were scanned with SEM. EDX analysis was done with an INCA instrument, (Oxford Instruments, England). EDX was used for elemental analysis to confirm that elements, such as silica nanoparticles, existed on the membranes.

FTIR analysis was used to detect the presence of functional groups in the fabricated composite membranes. An Nicolet 6700 FTIR spectrometer, (Thermo Fisher Scientific Inc., MA) with a DTGS KBr detector and a KBr beam splitter was used for FTIR analysis. In this study, there were two main compounds that needed to be tested with FTIR analysis: PSF and PVA. First, the PSF membrane with PVA was scanned with FTIR and then compared with the spectrum of PVA alone to verify the existence of PVA in the PSF membrane. Before the FTIR analysis, the membrane samples needed to be completely dried to prevent noises caused by moisture. All spectra were obtained from 32 scans at a 4.00-cm^{-1} resolution with wave numbers ranging from 400 to 4000 cm^{-1} and with an optical velocity of 0.6329.

TABLE II
CCD of the Experiments for Membranes Modified with PVA and Silicon Dioxide Nanoparticles

Run	Factors with coded levels		Responses	
	A: PVA (wt %)	*B:* SiO_2 (wt %)	Y_1 (L m^{-2} h^{-1} bar^{-1})	Y_2 (%)
1	0.00	0.00	13.07	48.15
2	0.00	1.41	38.36	71.87
3	1.00	−1.00	16.06	48.49
4	−1.00	−1.00	10.27	35.90
5	0.00	−1.41	7.59	36.63
6	−1.41	0.00	7.13	29.17
7	0.00	0.00	9.11	44.60
8	0.00	0.00	12.29	48.41
9	1.00	1.00	78.93	99.48
10	−1.00	1.00	28.22	74.79
11	0.00	0.00	15.20	54.53
12	1.41	0.00	20.24	66.64
13	0.00	0.00	7.21	35.24

Experimental design

The most popular RSM design is CCD. CCD is a method that can be efficiently applied to develop a second-order response model with a few numbers of factors n ($2 \leq n \leq 6$).[26] CCD has three groups of design points, which are two-level factorial or fractional factorial design points, axial points, and center points. Center points are usually repeated four to six times to get a good estimate of experimental error. In this case, we used the experimental CCD used for RSM of the membrane modification with two independent process variables, the PVA and silica nanoparticle weight percentages. There were five center points, four axial points, and four fractional factorial design points; this rendered a total of 13 runs of the experiment to analyze the data acquired from the experimental runs.

Table II, developed with Design Expert software (version 6.0.10, Stat-Ease, Inc, MN), shows CCD of the experiments with two input variables or factors and two responses were observed. In the data analysis, the mathematical model selected from CCD had the highest polynomial order with significant terms, and it was not aliased.[21]

RESULTS AND DISCUSSION

RSM and analysis of variance (ANOVA)

Membrane permeability

The effects of interaction between different weight percentages of PVA and silica nanoparticles toward membrane permeability were plotted graphically to ease visual analysis on the basis of the mathematical analysis of the experimental data. The three-dimensional response surface for membrane permeability is presented in Figure 1. The transformation of the membrane permeability data was done with the reciprocal square root mathematical function to meet the assumptions that made the ANOVA valid. By referring to the three-dimensional surface figure for membrane permeability, we observed that the increment of silica nanoparticles and PVA weight percentages led to an increase in the membrane permeability.

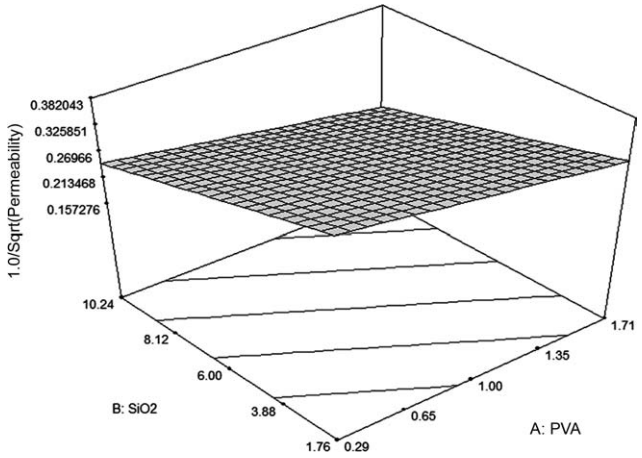

Figure 1 Three-dimensional response surface for membrane permeability (Sqrt = square root).

Also, the interaction plots were plotted to interpret two-factor interactions. They appear in the figure as two nonparallel lines and indicate that the effect of one factor depended on the level of the other. From the interaction plot in Figure 2, we observed that at high and low weight percentages of silica nanoparticles, the increment in the PVA weight percentage increased the membrane permeability. Moreover, both lines were almost parallel to each other, and thus, we postulated that the effect of the silica nanoparticle

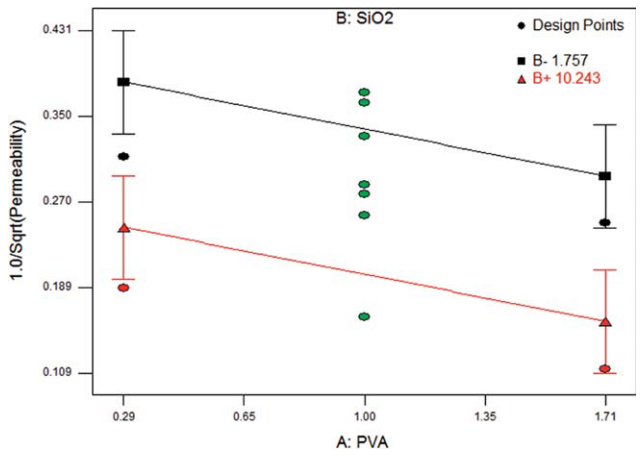

Figure 2 Interaction plot of the membrane permeability (Sqrt = square root). [Color figure can be viewed in the online issue, which is available at wileyonlinelibrary.com.]

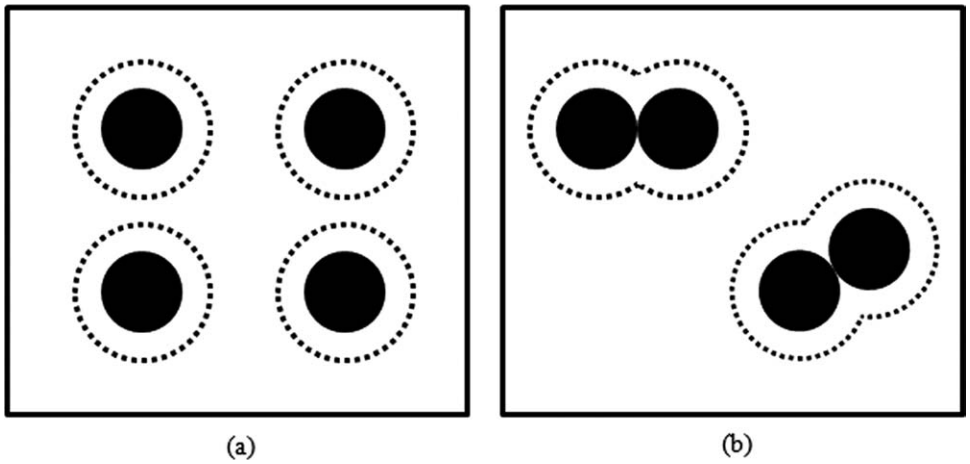

Figure 3 Nanogap formation in the PSF membranes: (a) well-dispersed and (b) agglomerated silica nanoparticles.

weight percentage was not dependent on the PVA weight percentage in affecting the PSF membrane permeability. The higher weight percentage of the silica nanoparticles may have increased the membrane permeability by the increment of the nanogap area formed. In a previous study,[27] the poor compatibility of the inorganic nanoparticle surface and the polymer prevented the polymer chains from contacting the inorganic nanoparticles and thus formed a narrow gap surrounding the inorganic particles. In addition to being used to stabilize nanoparticle surfaces to avoid agglomeration,[28] PVA has also been used as a pore former. Thus, an increase in the PVA weight percentage led to a significantly increase in the membrane permeability.

As shown in Figure 3, the black big dots are used to represent the nanoparticles. The empty areas between the line circles and the nanoparticles are the nanogaps formed. As shown in Figure 3(a), when the nanoparticles were well dispersed, the area of the nanogap was higher. Thus, a higher free volume was available to increase the permeability. However, when too many nanoparticles were added, a lot of agglomeration between the silica nanoparticles easily occurred. This caused a reduced area of nanogap, as shown in Figure 3(b), and thus, reduced the permeability at higher silica nanoparticle weight percentages. The nanogap formation due to silica nanoparticles was observed in the SEM pictures captured of the separation surface layer and cross sections of the membranes.

Generally, PSF membrane permeability was affected by the weight percentages of PVA and silica nanoparticles, according to the membrane permeability model in terms of the coded factors or in terms of the actual factors, as shown:

$$\frac{1}{\sqrt{Y_1}} = 0.27 - 0.044(A) - 0.068(B)$$

$$\frac{1}{\sqrt{Y_1}} = 0.42859 - 0.062471(\text{PVA}) - 0.016077(\text{SiO}_2)$$

where Y_1 is the permeability. Table III shows the ANOVA for the regression models and model terms. It was obvious from the results that there was no major interaction between the independent factors A and B. This also indicates that the experimental results fit well into the model with a value of $p > F < 0.05$. Values of R^2 (0.6446) and the standard deviation (0.054) showed the reliability of the regression models for membrane permeability. The regression value of the model showed that the data represented could be fitted satisfactorily into the model with moderate accuracy. The reason moderate accuracy was achieved was that all the membranes prepared were cast manually without the help of any casting machine. As a result, the casting speed was not constant in each membrane preparation. Thus, there were variations in the thickness of the membranes prepared; these highly affected the performances of the membranes.

TABLE III
ANOVA for the Permeability Regression Models and Model Terms

Source	Sum of squares	DF	Mean square	F	$p > F$	
Model	0.052831312	2	0.026415656	9.070017261	0.0057	Significant
A	0.015610536	1	0.015610536	5.359996963	0.0431	Significant
B	0.037220775	1	0.037220775	12.78003756	0.0051	Significant
Lack of fit	0.020346954	6	0.003391159	1.545440526	0.3507	Not significant

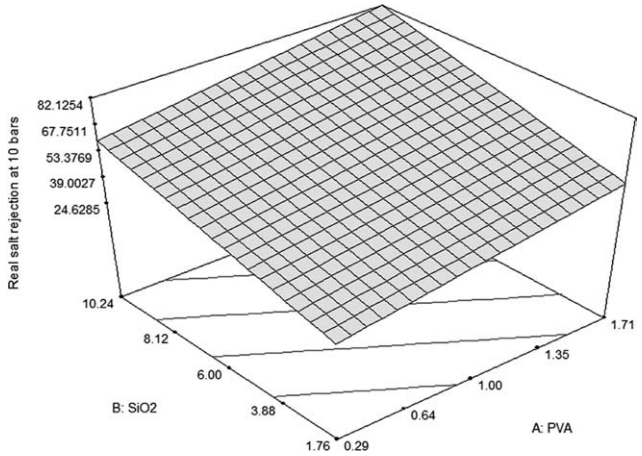

Figure 4 Three-dimensional response surface for R_{real} of the membrane.

R_{real} of the membrane

In the salt rejection process, a concentration of polarization can easily occur and cause a lower R_{obs}. Thus, all of the rejection data was interpreted in terms of R_{real}, which took into account concentration polarization, as opposed to R_{obs}, which is the experimentally measured rejection.[29]

To ease the visual analysis of R_{real} (Na_2SO_4) of the membrane at 10 bars, a three-dimensional response surface graph is plotted in Figure 4. This three-dimensional graph was plotted on the basis of the mathematical analysis of the R_{real} data at 10 bars. No transformation of the data was required because all of the data met the assumptions that made the ANOVA valid. As shown in the three-dimensional response surface graph, increases in the content of PVA and silica nanoparticles led to an increase in R_{real} at 10 bars.

The interaction plot of the effects of the PVA and silica nanoparticle weight percentages on R_{real} at 10 bars is shown in Figure 5. An increase in PVA caused an increase in R_{real} at 10 bars at both high and low weight percentages of silica nanoparticles. The lines indicating the condition of high and low weight percentages of silica nanoparticles were almost parallel to each other. Thus, we postulated from this interaction plot that the effect of PVA was independent of the level of the silica nanoparticles in affecting R_{real} at 10 bars. In other words, an increase in the PVA or silica nanoparticle weight percentage in the PSF membrane could increase R_{real} at 10 bars. The flux increment in the modified PSF membrane did not decrease or lower the ability of the membranes to reject the Na_2SO_4 salt permeation through the membranes.

The real salt rejection of the membrane at 10 bars (Y_2) could be represented by the model in terms of the coded factors or in terms of the actual factors, as shown:

$$Y_2 = 53.38 + 11.28(A) + 17.46(B)$$

$$Y_2 = 12.72050 + 15.95774(\text{PVA}) + 4.11645(\text{SiO}_2)$$

For R_{real} at 10 bars for the modified PSF membrane, only two terms were considered significant from the statistical analysis. A combination of these significant terms contributed to a linear empirical model for the membrane R_{real}. The reliability level of the generated linear model was verified through the value of R^2 (0.7271) and a standard deviation of 11.39. ANOVA for regression models and the model terms shown in Table IV indicated that there was no major interaction between the independent factors A and B because both of them were significant factors. The experimental results for R_{real} fit well into this linear model; this was further verified by the value of $p > F = 0.0015$, which was less than 0.05. Also, the lack of fit for this model was 0.1156, which was not significant.

Optimization of the membrane composition

The membrane fabrication was run with optimized composition generated by the regression analysis. The ultimate goal was to produce a membrane with the maximum permeability and highest salt rejection. The predicted values were compared with the actual values obtained after the confirmation run. Optimization was done to maximize the permeability value of the membrane and the R_{real} value of the membrane.

The errors of the data were calculated on the basis of the following equation:

$$\text{Error}(\%) = \left(\frac{\text{Actual value} - \text{Predicted value}}{\text{Actual value}}\right) \times 100\%$$

This confirmation run was conducted at a composition of 1.71 wt % PVA and 10.24 wt % silica

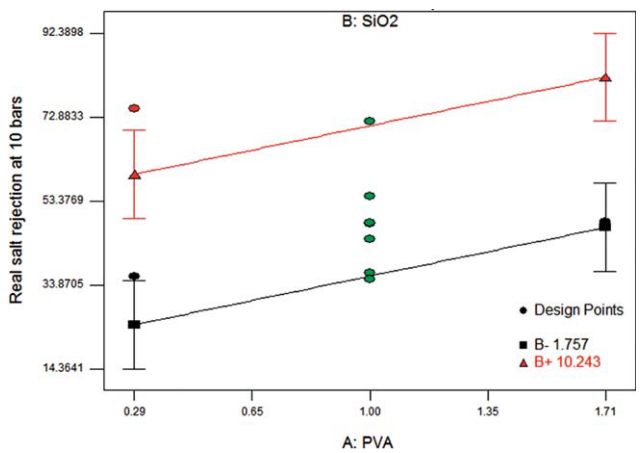

Figure 5 Interaction plot of R_{real} of the membrane. [Color figure can be viewed in the online issue, which is available at wileyonlinelibrary.com.]

TABLE IV
ANOVA for R_{real} Regression Models and Model Terms

Source	Sum of squares	DF	Mean square	F	$p > F$	
Model	3458.698278	2	1729.349139	13.32030128	0.0015	Significant
A	1018.597251	1	1018.597251	7.845739163	0.0188	Significant
B	2440.101027	1	2440.101027	18.7948634	0.0015	Significant
Lack of fit	1097.524679	6	182.9207798	3.644636683	0.1156	Not significant

nanoparticles with a desirability of 0.79. As shown in Table V, the permeability value from the confirmation run was 61.926 L m^{-2} h^{-1} bar^{-1}, and R_{real} was 97.5850%. From this preliminary study, we observed that the composition of PVA and silica nanoparticles could be optimized and improved the permeability and R_{real} of the PSF membrane. The actual membrane permeability with a 34.72% error and membrane R_{real} with a 15.84% error after optimization compared with the predicted value could be considered as acceptable and reasonable. The error between the predicted and actual value might have been due to uncontrolled parameters, such as the membrane casting speed, contact time in air before the phase-immersion process, and temperature variation of the phase-inversion medium. For future work, these factors should be investigated in depth to correlate their effects on the membrane permeability and R_{real} to reduce the error between the predicted and actual values.

SEM analysis

SEM of the composite membrane samples is shown in Figure 6. Different membrane composition from run orders 5, 6, and 9 were selected to undergo scanning to investigate the effect of PVA on the PSF membrane, the effect of the silica nanoparticles on the PSF membrane, and the effect of a combination of both PVA and silica nanoparticles on the PSF membrane. The membranes from run orders 5, 6, and 9 were labeled as runs 5, 6, and 9 in the SEM micrographs.

The SEM results for the separation layer of the composite membranes from runs 5, 6, and 9 were scanned and are shown in Figure 6(a,c,e), respectively. These membranes were selected for SEM scanning to provide a better view on the separation surface. When the membrane was modified with only PVA (run 5), the PSF membrane surface had more pores [Fig. 6(a)] compared with membrane modified with only silica nanoparticles [run 6; Fig. 6(c)]. However, the combination of both PVA and silica nanoparticles created pores occupied by the silica nanoparticles [Fig. 6(e)].

An increase in the PVA or silica nanoparticle weight percentage increased the membrane permeability and R_{real}. This observation was due to the formation of more pores as a result of the additives. However, the combination of both the PVA and silica nanoparticles produced pores with larger nanogaps. These nanogaps increased the permeability of the membranes and, at the same time, maintained its capability to reject salts because of the silica nanoparticles, which occupied the pores and rejected the passage of the salt ions. From our observations, the PSF membranes modified with silica nanoparticles and PVA had higher R_{real} and higher permeability values.

By comparing the SEM micrographs at the same magnification of 5000×, we observed no apparent differences among all of the membrane cross sections. Both of them showed a typical asymmetric morphology with fingerlike pores linked by sponge walls. These findings indicate that the addition of PVA and silica nanoparticles did not affect the structures of the membrane cross sections. Therefore, the mechanism of PSF membrane structure formation was not altered by the addition of PVA or silica nanoparticles.

However, the membrane from the run 9 cross section [Fig. 6(f)] showed wider cavities at a location far from the membrane top surface. The small diameter of cavities at the membrane top surface of run 9 and the large cavity diameter at the bottom of the membrane, which was few times larger compared with that of cavities at the membrane top surface, could be used to explain the increase in the membrane permeability dramatically with the maintenance of the membrane's ability to reject salt permeation.

Contact angle test

We observed in the SEM micrographs that the agglomeration of inorganic nanoparticles could not be avoided completely. This was due to the fact that when the size of the particles was reduced to the

TABLE V
Confirmation Runs for the Permeability and R_{real} Tests

	Permeability (L m^{-2} h^{-1} bar^{-1})	R_{real} at 10 bars (%)
Predicted value	40.4273	82.1253
Actual value	61.9260	97.5850
Error (%)	34.72	15.84

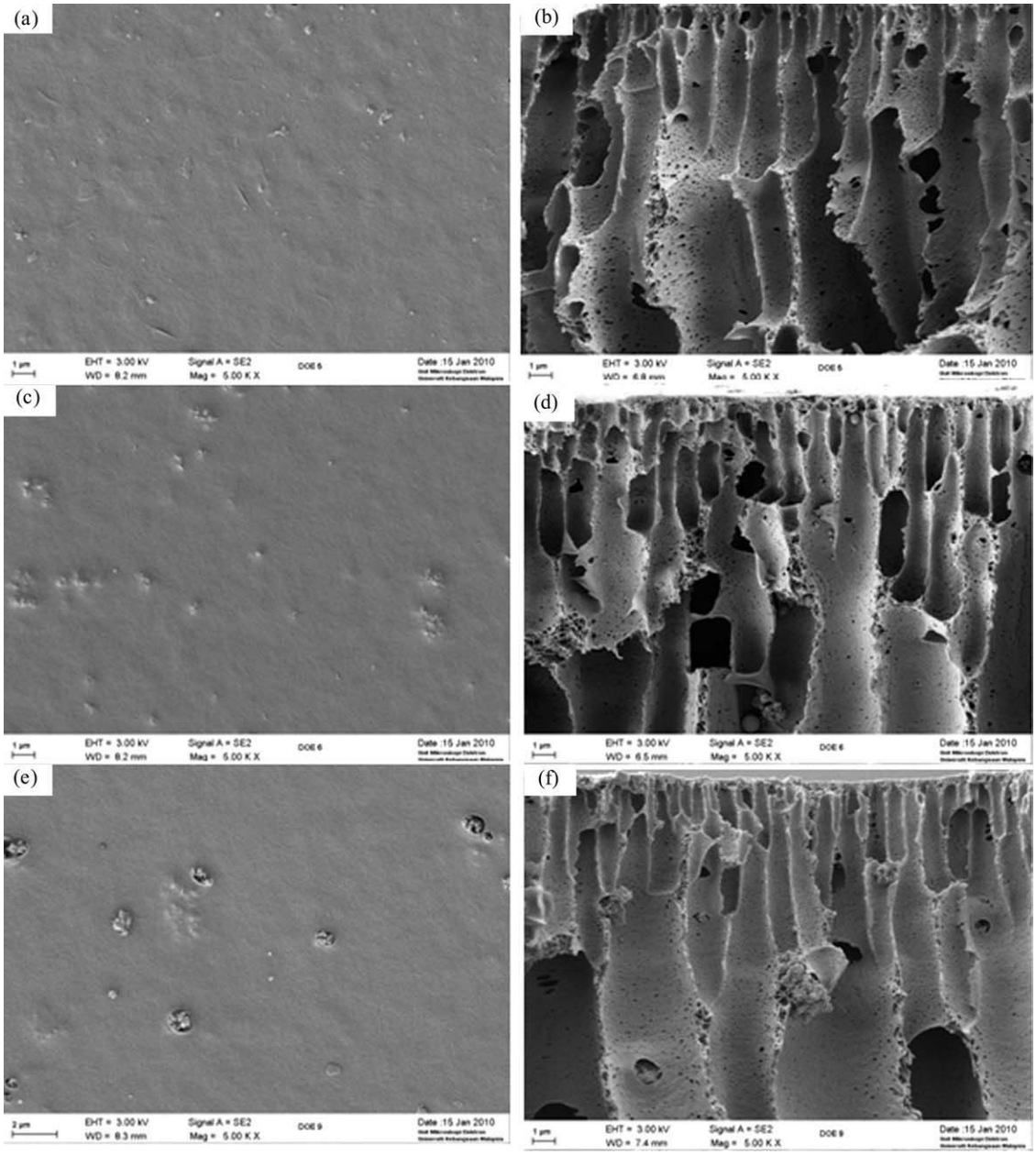

Figure 6 SEM micrograph of the separation layer and cross section of the composite membrane sample: runs (a,b) 5, (c,d) 6, and (e,f) 9.

nanolevel, the ratio of surface to bulk atoms increased and thereby increased the energy of the system as a whole; this led to a decrease in the system stability. The nanoparticles tended to be attracted to each other through van der Waals forces and led to the agglomeration and corresponding reduction in the surface energy.[28] The reduction in the surface energy then caused an increase in the contact angle value, as reported by others.[30,31]

As shown by the contact angle three-dimensional plot in Figure 7, we observed that at a low weight percentage of PVA, an increase in silica nanoparticles led to an increase in the contact angle values. In other words, an increase in the silica nanoparticles caused an increase in the membrane hydrophobicity. This could be explained by the fact that the increase in the silica nanoparticle weight percentage caused more agglomeration to occur between the nanoparticles and, thus, reduced the surface energy of the membrane itself; this led to an increase in the contact angle of the PSF membranes.

However, at a high PVA weight percentage, we observed that the PSF membrane contact angle was reduced dramatically, even at a high weight percentage of silica nanoparticles. This significant finding was attributed to the fact that PVA itself is a hydrophilic material.[19,32] Also, PVA was important in stabilizing the nanoparticle surface, a phenomena

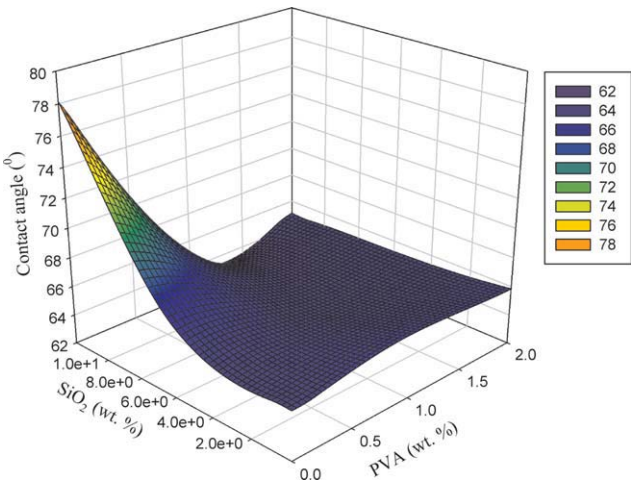

Figure 7 Effects of the silicon dioxide nanoparticles and PVA weight percentages on the membrane contact angle. [Color figure can be viewed in the online issue, which is available at wileyonlinelibrary.com.]

called *steric stabilization.*[28] PVA could stabilize nanoparticle surfaces against aggregation through the presence of long-chain hydrocarbons in their structure. So, we concluded that the use of PVA prevented the agglomeration of silica nanoparticles and, thus, prevented the increase in the hydrophobicity of the PSF membranes.

Tensile strength test

The tensile strength test was conducted to study the mechanical properties of the fabricated membranes. Membranes with better mechanical properties are more desired for a wider span of applications with higher performance. Generally, an increase in silica nanoparticles increases the tensile strength of the PSF membrane because the free motion of polymeric chains is partly restricted by intermolecular forces between the polymeric chains and inorganic oxide nanoparticles.[2] The same observation was made in this study.

As shown in the three-dimensional tensile strength plot in Figure 8, at low silica nanoparticle weight percentages, an increase in PVA reduced the tensile strength of the PSF membrane. This showed that PVA possessed a weakening effect on the PSF membranes. However, at higher silica nanoparticle weight percentages, an increase in PVA increased the tensile strength of the PSF membranes up to around 1 wt % PVA. This might have been due to the fact that when more PVA was added, the silica nanoparticles were better dispersed because of steric stabilization.[28] Thus, more restriction was imposed on the free motion of polymeric chains, and as a result, the tensile strength of the PSF membrane was increased. However, a further increase in PVA at a high silica nanoparticle weight percentage no longer increased the tensile strength of the PSF membrane because of the weakening effect of PVA itself.

EDX analysis

EDX mapping mode was used to study the distribution of overall chemical elements of interest in the membranes. In this case, EDX was done to check the distribution of silica nanoparticles in the PSF membrane with and without PVA. We postulated that PVA would reduce the agglomeration of silica nanoparticles in the PSF membranes.

EDX spectroscopy was performed on two PSF membranes with the same weight percentage of silica nanoparticles, 10.24 wt %. However, to one of the PSF membranes was added 1.71 wt % PVA, and no PVA was added to the other one.

Figure 9 shows the captured images of the membrane surfaces with the silicon element distribution maps. Red color dots are used to represent the distribution of the silicon element on the membrane surfaces. The silica nanoparticles in the membrane with PVA [Fig. 9(b)] showed a better distribution with less agglomeration.

FTIR spectroscopy analysis

FTIR analysis has been applied in many previous studies because of its accuracy and reliable results in verifying the existence of certain chemical compounds, especially organic chemical compounds. As shown in Figure 10, there were two observable absorption peaks for pure PSF at wave numbers around 1290 and 1325 cm^{-1} due to the symmetric O=S=O stretching vibration; this result is

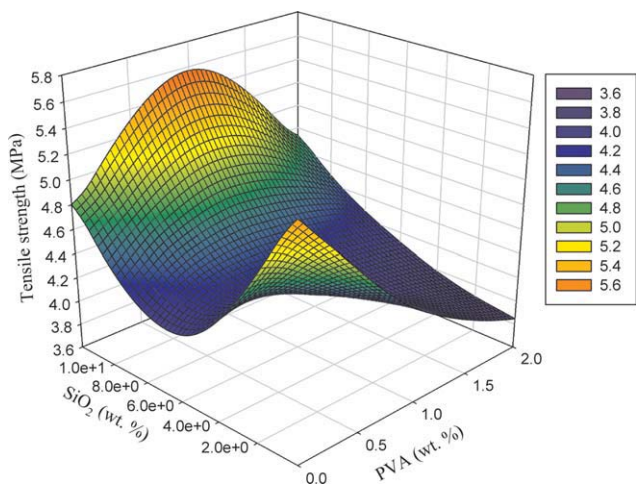

Figure 8 Effects of the silicon dioxide nanoparticles and PVA weight percentages on the membrane tensile strength. [Color figure can be viewed in the online issue, which is available at wileyonlinelibrary.com.]

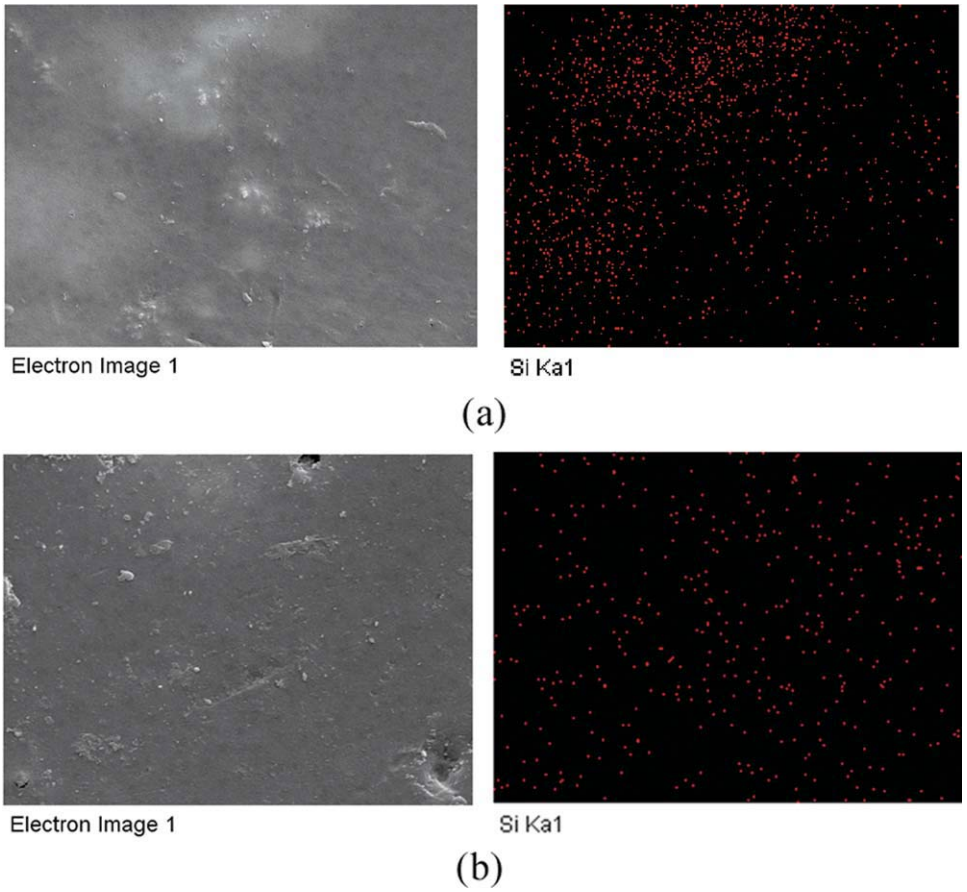

Figure 9 EDX spectrum for the silica-nanoparticle-incorporated membranes (a) without and (b) with PVA.

comparable with those of previous studies.[2] Also, another absorption peak was observed around a wave number of 1600 cm^{-1}; this was caused by the rotation of the C=C conjugation system of the benzene ring. The presence of another absorption peak at a wave number of 3000 cm^{-1} was due to the asymmetric —CH_3 stretching vibration. From previous works,[2] the absorption peak of —OH at the wave number of 3400 cm^{-1} was observed for pure PSF membrane due to the incomplete drying process. However, as shown in Figure 10, an absorption peak for —OH was not observed, and we postulated that the membrane sample fully underwent the drying processes.

The FTIR spectrum obtained for pure PVA exhibited the characteristic C—H stretching at 2914 and 2820 cm^{-1} and O—H stretching at 3428 cm^{-1}. Also, there was a stronger absorption peak from 1060 to 1100 cm^{-1}; this was assigned as the absorption peak of C—O—C of the crosslinked PVA. All of these results were comparable with those of a previous analysis of pure PVA.[33]

Thus, a combination of pure PVA and the PSF membrane produced the FTIR spectrum shown in Figure 10. The spectrum exhibited characteristic groups from both pure PVA and the PSF membrane. As a result, we concluded that PVA fit well in the PSF membrane structure, as predicted.

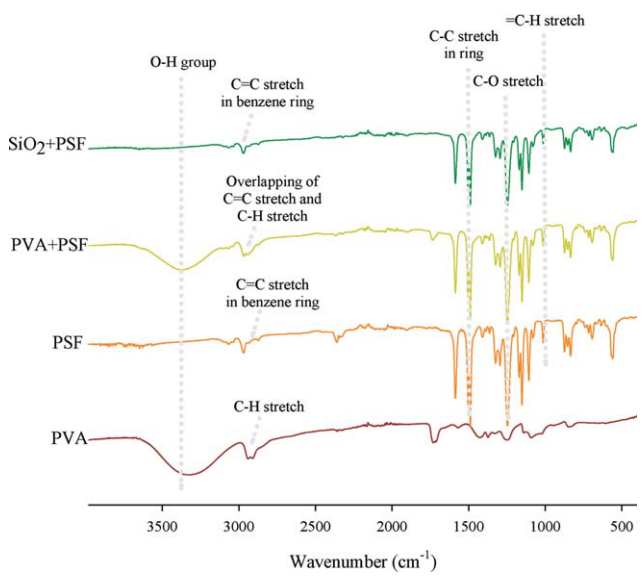

Figure 10 FTIR analysis for PVA, PSF, PSF with PVA, and PSF with SiO_2. [Color figure can be viewed in the online issue, which is available at wileyonlinelibrary.com.]

CONCLUSIONS

On the basis of the response surface plots, different weight percentages of PVA and silica nanoparticles significantly affected the membrane permeability and salt rejection. Silica nanoparticles were the major factor affecting the PSF membrane permeability. However, both of the factors were found to be significant in affecting the salt rejection of the PSF membranes. Empirical models obtained from statistical analysis were used in the prediction of the respective responses for the process optimization. The optimum composition obtained from CCD was 1.71 wt % PVA with 10.24 wt % silica nanoparticles in the PSF membrane. This composition was the optimum level in which R_{real} and the permeability of the PSF membrane reached the highest possible values. The permeability and R_{real} obtained experimentally were 61.9260 L m^{-2} h^{-1} bar^{-1} and 97.5850%, respectively, where their deviations from the predicted values were 34.72 and 15.84%, respectively. From the membrane characterization, we observed that the addition of PVA prevented the agglomeration of silica nanoparticles and, thus, prevented the increase in the hydrophobicity of the PSF membranes. Furthermore, the tensile strength test confirmed that the addition of silica nanoparticles increased the mechanical properties of the PSF membranes. However, addition of PVA caused a weakening effect on the mechanical properties of the PSF membrane. Also, EDX and FTIR testing confirmed that the silica nanoparticles and PVA were well incorporated and blended with the PSF membranes.

References

1. Sivakumar, M.; Mohan, D. R.; Rangarajan, R. J Membr Sci 2006, 268, 208.
2. Zhang, Y.; Shan, L.; Tu, Z.; Zhang, Y. Sep Purif Technol 2008, 63, 207.
3. Yoo, J. E.; Kim, J. H.; Kim, Y.; Kim, C. K. J Membr Sci 2003, 216, 95.
4. Kim, K. S.; Lee, K. H.; Cho, K.; Park, C. E. J Membr Sci 2002, 199, 135.
5. Zeng, G.-M.; Xu, K.; Huang, J.-H.; Li, X.; Fang, Y.-Y.; Qu, Y.-H. J Membr Sci 2008, 310, 149.
6. Zularisam, A. W.; Ismail, A. F.; Salim, M. R.; Sakinah, M.; Hiroaki, O. J Membr Sci 2007, 299, 97.
7. Torto, N.; Laurell, T.; Gorton, L.; Varga, G. M. J Membr Sci 1997, 130, 239.
8. Bowen, R. W.; Doneva, T. A.; Yin, H. B. J Membr Sci 2001, 181, 253.
9. Kim, S. R.; Lee, K. H.; Jhon, M. S. J Membr Sci 1996, 119, 59.
10. Chen, S.-H.; Liou, R.-M.; Lin, Y.-Y.; Lai, C.-L.; Lai, J.-Y. Eur Polym J 2009, 45, 1293.
11. Bryjak, M.; Gancarz, I.; Pozniak, G.; Tylus, W. Eur Polym J 2002, 38, 717.
12. Bottino, A.; Capannelli, G.; Comite, A. Desalination 2002, 146, 35.
13. Yan, L.; Li, Y. S.; Xiang, C. B.; Xianda, S. J Membr Sci 2006, 276, 162.
14. Yang, Y.; Zhang, H.; Wang, P.; Zheng, Q.; Li, J. J Membr Sci 2007, 288, 231.
15. Chiang, P. C.; Whang, W. T. Polymer 2003, 44, 2249.
16. Faibish, R. S.; Cohen, Y. J Membr Sci 2001, 185, 129.
17. Ahn, J.; Chung, W.-J.; Pinnau, I.; Guiver, M. D. J Membr Sci 2008, 314, 123.
18. Jadav, G. L.; Singh, P. S. J Membr Sci 2009, 328, 257.
19. Yang, J. M.; Chiang, C. Y.; Wang, H. Z.; Yang, C. C. J Membr Sci 2009, 341, 186.
20. Xiangli, F.; Wei, W.; Chen, Y.; Jin, W.; Xu, N. J Membr Sci 2008, 311, 23.
21. Montgomery, D. C. Design and Analysis of Experiments; Wiley: Hoboken, NJ, 2001.
22. Skluzacek, J. M.; Isabel Tejedor, M.; Anderson, M. A. Micropor Mesopor Mater 2006, 94, 288.
23. Hilal, N.; Mohammad, A. W.; Atkin, B.; Darwish, N. A. Desalination 2003, 157, 137.
24. Mohammad, A. W.; Hilal, N.; Al-Zoubi, H.; Darwish, N. A. J Membr Sci 2007, 289, 40.
25. Zodrow, K.; Brunet, L.; Mahendra, S.; Li, D.; Zhang, A.; Li, Q.; Alvarez, P. J. J. Water Res 2009, 43, 715.
26. Khayet, M.; Seman, M. N. A.; Hilal, N. J Membr Sci 2010, 349, 113.
27. Cong, H.; Radosz, M.; Towler, B. F.; Shen, Y. Sep Purif Technol 2007, 55, 281.
28. Pradeep, T.; Anshup. Thin Solid Films 2009, 517, 6441.
29. Bowen, W. R.; Mukhtar, H. J Membr Sci 1996, 112, 263.
30. Mykhaylyk, T. A.; Evans, S. D.; Fernyhough, C. M.; Hamley, I. W.; Henderson, J. R. J Colloid Interface Sci 2003, 260, 234.
31. Tan, K.; Obendorf, S. K. J Membr Sci 2006, 274, 150.
32. Vijaya Kumar Naidu, B.; Sairam, M.; Raju, K. V. S. N.; Aminabhavi, T. M. J Membr Sci 2005, 260, 142.
33. Gong, J.; Luo, L.; Yu, S.-H.; Qian, H.; Fei, L. J Mater Chem 2006, 16, 101.